



HAL
open science

Enhanced extreme wave statistics of irregular waves due to accelerating following current over a submerged bar

Jie Zhang, Yuxiang Ma, Ting Tan, Guohai Dong, Michel Benoit

► To cite this version:

Jie Zhang, Yuxiang Ma, Ting Tan, Guohai Dong, Michel Benoit. Enhanced extreme wave statistics of irregular waves due to accelerating following current over a submerged bar. *Journal of Fluid Mechanics*, 2023, 954, pp.A50. 10.1017/jfm.2022.1022 . hal-03932053

HAL Id: hal-03932053

<https://hal.science/hal-03932053>

Submitted on 10 Jan 2023

HAL is a multi-disciplinary open access archive for the deposit and dissemination of scientific research documents, whether they are published or not. The documents may come from teaching and research institutions in France or abroad, or from public or private research centers.

L'archive ouverte pluridisciplinaire **HAL**, est destinée au dépôt et à la diffusion de documents scientifiques de niveau recherche, publiés ou non, émanant des établissements d'enseignement et de recherche français ou étrangers, des laboratoires publics ou privés.

Banner appropriate to article type will appear here in typeset article

Enhanced extreme wave statistics of irregular waves due to accelerating following current over a submerged bar

Jie Zhang¹, Yuxiang Ma^{†1}, Ting Tan¹, Guohai Dong¹, Michel Benoit^{2,3}

¹State Key Laboratory of Coastal and Offshore Engineering, Dalian University of Technology, Dalian 116023, PR China

²EDF R&D, Laboratoire National d'Hydraulique et Environnement (LNHE), Chatou, France

³Saint-Venant Hydraulics Laboratory (Ecole des Ponts ParisTech, EDF R&D), Chatou, France

(Received xx; revised xx; accepted xx)

We present experimental results of irregular long-crested waves propagating over a submerged trapezoidal bar with the presence of a background current in a wave flume. We investigate the non-equilibrium phenomenon (NEP) induced by significant changes of water depth and mean horizontal flow velocity as the wave trains pass over the bar. Using statistical moments skewness and kurtosis as proxies, we show evidence that an accelerating following current could increase the sea-state non-Gaussianity and enhance both the magnitude and spatial extent of NEP. We also find that below a “saturation relative water depth” $k_p h_2 \approx 0.5$ (k_p being the peak wave number in the shallow area of depth h_2), although the NEP manifests, the decrease of the relative water depth does not further enhance the maximum skewness and kurtosis over the bar crest. This work highlights the nonlinear physics according to which a following current could provoke higher freak wave risk in coastal areas where the modulation instability plays an insignificant role.

Key words:

1. Introduction

Extreme waves with crest-to-trough excursions higher than twice the significant wave height are referred to as “freak waves” or “rogue waves” (see e.g. Dysthe *et al.* 2008). Although different mechanisms have been put forward (Kharif & Pelinovsky 2003; Onorato *et al.* 2013; Adcock & Taylor 2014), the universal explanation of freak wave formation in the context of ocean waves is still under debate (Akhmediev & Pelinovsky 2010; Fedele *et al.* 2016; Dematteis *et al.* 2019).

As a new perspective of nonlinear focusing, the non-equilibrium dynamics (NED) provoked by an abrupt change of environmental conditions has received considerable attention in the last years (see e.g. Onorato & Suret 2016; Trulsen 2018). It renders some generality in

[†] Email address for correspondence: yuxma@dlut.edu.cn

33 explaining the freak wave formation in coastal areas, where the well-known modulation
34 instability (MI) introduced by Benjamin (1967) may be restrained (Voronovich *et al.* 2008;
35 Kharif *et al.* 2010). The pioneering investigation of NED effects induced by significant depth
36 change was conducted by Trulsen *et al.* (2012). Using skewness and kurtosis as proxies, they
37 showed that the non-Gaussian behaviour and freak wave occurrence probability are locally
38 enhanced shortly after a submerged slope. Recent studies have investigated various factors
39 affecting the sea-state non-equilibrium responses. The relative water depth in the shallower
40 area plays the dominant role (Zeng & Trulsen 2012; Trulsen *et al.* 2020): it should be lower
41 than a threshold for the NED to manifest. Other factors, including the incident significant
42 wave height (Zheng *et al.* 2020; Zhang *et al.* 2022), the spectral width (Ma *et al.* 2015), the
43 wave direction (Ducrozet & Gouin 2017; Ma *et al.* 2017), and the shape of the bathymetry
44 (Gramstad *et al.* 2013; Kashima & Mori 2019; Zheng *et al.* 2020; Lawrence *et al.* 2022)
45 also influence the sea-state dynamical responses. For the out-of-equilibrium sea-states, the
46 wave kinematics (Lawrence *et al.* 2021; Zhang & Benoit 2021) as well as the sea-state
47 equilibration process in long spatial scale (Zhang *et al.* 2019, 2022) have been studied. From
48 a theoretical perspective, the intensified freak wave probability provoked by significant depth
49 variations could be described by the stochastic model of Li *et al.* (2021*b*) which is built based
50 on the second-order deterministic model (Li *et al.* 2021*a,c*), or by the stochastic model for
51 non-homogeneous processes introduced in Mendes *et al.* (2022).

52 In addition to bathymetry variations, currents and tides play significant roles in the wave
53 evolution in coastal areas (Longuet-Higgins & Stewart 1961; Peregrine 1976), and could lead
54 to freak wave formation (Lavrenov & Porubov 2006). Here, we limit ourselves to discuss
55 the case of horizontally non-homogeneous currents without evident vertical shear effect (i.e.
56 the mean horizontal flow velocity varies in the horizontal direction x , yet the profile of
57 the horizontal velocity remains more or less uniform in the vertical direction). The sheared
58 currents as well as the current-induced vorticity are important for freak wave formation (see
59 e.g. Hjelmervik & Trulsen 2009; Curtis & Murphy 2020), and are left for future investigation.

60 In the linear regime, the adverse current could refract waves and form spatial wave
61 focusing locations (caustics), such freak waves can be well predicted by the ray theory
62 (White & Fornberg 1998). In the nonlinear regime, ambient currents could change the freak
63 wave probability via affecting the wave steepness. When propagating over a current with
64 adverse gradient in the horizontal velocity (i.e., accelerating opposing current or decelerating
65 following current), wave steepness is enhanced. The wave nonlinearity is therefore increased,
66 promoting the destabilization of the wave train (Gerber 1987; Stocker & Peregrine 1999),
67 and the occurrence of a frequency downshift (Chawla & Kirby 2002; Ma *et al.* 2010).
68 Furthermore, the criterion for the manifestation of MI is altered due to the current (Liao *et al.*
69 2017), so that MI may occur in wave trains that are considered stable in quiescent water. The
70 role of an opposing current on triggering freak waves as results of MI has been confirmed for
71 long-crested deep water waves (Onorato *et al.* 2011; Toffoli *et al.* 2013; Ducrozet *et al.* 2021),
72 and for short-crested waves over opposing currents that are either normal or oblique to the
73 mean wave propagation direction (Toffoli *et al.* 2011, 2015). However, MI ceases to manifest
74 anyway below the threshold depth that is corrected by considering the current effects, so that
75 the wave-current interaction as a nonlinear mechanism of freak wave formation becomes
76 ineffective for coastal waves and currents in sufficiently shallow water.

77 Most studies attribute the enhanced freak wave probability to the MI reinforced by opposing
78 currents, and consider that following currents would reduce the freak wave probability as
79 they weaken the MI. But this conclusion deserves to be investigated in the circumstances
80 where the MI does not dominate the wave evolution. In analogue to the depth variation,
81 the inhomogeneity of the current field may also result in NED (Trulsen 2018) and increase
82 the freak wave probability, but there is no experimental evidence of this mechanism yet.

No.	Upstream flat area (UWO/UWC)				Bar crest area (UWO/UWC)			
	T_p (s)	H_s (cm)	μ	ϵ	T_p (s)	H_s (cm)	μ	ϵ
1	1.38/1.38	5.6/4.9	2.18/2.00	0.043/0.034	1.38/1.38	5.0/3.9	1.07/0.90	0.047/0.031
2	1.48/1.49	6.6/5.8	1.91/1.76	0.044/0.036	1.49/1.50	5.9/4.8	0.97/0.82	0.050/0.035
3	1.60/1.60	6.4/5.8	1.69/1.58	0.038/0.032	1.60/1.60	5.8/4.8	0.88/0.76	0.045/0.032
4	1.79/1.78	7.3/6.5	1.41/1.35	0.036/0.031	1.81/1.80	6.7/5.6	0.76/0.67	0.045/0.033
5	2.12/2.14	9.0/8.4	1.11/1.05	0.036/0.031	2.15/2.17	8.7/7.5	0.63/0.54	0.048/0.036
6	2.24/2.27	9.1/8.7	1.03/0.97	0.033/0.030	2.27/2.30	8.8/7.9	0.59/0.51	0.046/0.035
7	2.35/2.38	9.2/8.7	0.97/0.92	0.031/0.028	2.39/2.41	8.8/8.0	0.56/0.48	0.043/0.034
8	2.45/2.48	11.0/10.8	0.92/0.87	0.036/0.033	2.50/2.51	10.8/10.1	0.53/0.46	0.051/0.041
9	2.54/2.57	10.2/10.2	0.88/0.83	0.032/0.030	2.57/2.58	10.0/9.6	0.51/0.45	0.046/0.038
10	2.86/—	10.0/—	0.76/—	0.027/—	2.89/—	10.0/—	0.45/—	0.040/—
11	3.17/—	7.9/—	0.68/—	0.019/—	3.16/—	8.1/—	0.41/—	0.030/—

Table 1: Key parameters in the UWO/UWC tests over the upstream flat area ($h_1 = 1$ m) and the bar crest area ($h_2 = 0.4$ m). The peak period T_p and significant wave height H_s are averaged measurements in each corresponding area. The wave number k_p is computed with the proper dispersion relationship (i.e. considering the local horizontal current velocity, if present).

83 In this study, we show experimental results of unidirectional irregular waves propagating
84 over horizontally non-homogeneous media, where the water depth and the following current
85 velocity change in the direction of wave propagation. Our main goal is to provide experimental
86 evidence that an accelerating following current can lead to NED and, counter-intuitively,
87 increase the freak wave occurrence without the effects of MI. In addition, we further discuss
88 the saturation relative water depth for enhancing the magnitude of NED.

89 The remainder of this article is organized as follows: the experimental setup and test
90 conditions are described in Section 2. The experimental results are analyzed in Section 3,
91 discussing the effects induced by the accelerating following current, and the evolution of the
92 maximum values of the statistical wave parameters achieved over the bar crest as functions
93 of relative water depth. Conclusions are summarized in Section 4.

94 2. Experimental setup

95 The experiments were conducted in the wave-current flume of the National Marine Environ-
96 mental Monitoring Center in Dalian, China. The flume, with total length $l = 80$ m and width
97 $b = 1.5$ m, is equipped with a piston-type wave maker on one side, and a passive dissipation
98 zone on the other. The current is generated with a pump, and the flow inlet is placed 2 m
99 after the wave maker, the outlet 1 m before the damping zone.

100 Four experimental configurations are considered hereafter. The two main ones are done
101 with a submerged trapezoidal bar and irregular waves, without any current (denoted UWO for
102 “Uneven bottom with Waves Only”) or with a following current (denoted UWC for “Uneven
103 bottom with Waves and Current”). Additional tests were conducted with the bar and only
104 the following current (denoted UCO for “Uneven bottom with Current Only”) for validation.
105 Finally, wave tests with the bar removed and no current (denoted FWO for “Flat bottom with
106 Waves Only”) were performed for comparative purpose.

107 The water depth close to the wave maker is fixed $h_1 = 1$ m throughout the campaign. The
108 submerged bar starts 17.3 m away from the wave maker, and consists of a 18 m long up-slope
109 (1/30), a 10 m long bar crest, and a 12 m long down-slope (−1/20). The origin of the x
110 abscissa is defined at the toe of the up-slope. Over the bar crest, the water depth is decreased

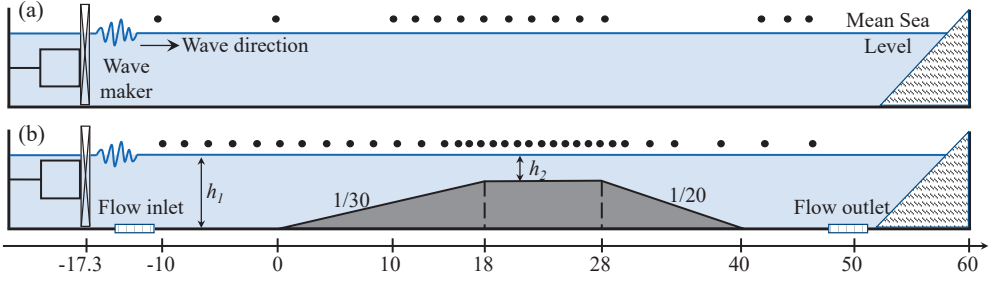


Figure 1: Sketch of the experimental setups and the locations of wave probes (solid black dots) for (a) the FWO tests, (b) the UCO, UWO and UWC tests.

111 to $h_2 = 0.4$ m. The relatively mild up-slope is chosen to diminish the vorticity of the flow that
 112 could be generated by the depth variation. The waves were measured by capacitance-type
 113 probes with sampling frequency 50 Hz. In the UWO and UWC tests, 33 wave probes were
 114 set with 2 m spacing before and over the up-slope, 1 m spacing close to the bar crest and
 115 4 m spacing after the bar. In the FWO tests, 16 probes were arranged with 2 m spacing in
 116 the area where the bar was installed. The layout of the two seabed configurations and the
 117 corresponding arrangements of the probes are shown in Fig. 1.

118 The incident wave trains are generated considering a JONSWAP-type spectrum $S(f)$:

$$119 \quad S(f) = \frac{\alpha g^2}{(2\pi)^4 f^5} \exp \left[-\frac{5}{4} \left(\frac{f_p}{f} \right)^4 \right] \gamma^{\exp \left[-(f-f_p)^2 / (2\sigma_J^2 f_p^2) \right]}, \quad (2.1)$$

120 where g denotes the acceleration of gravity, α controls the significant wave height, and
 121 σ_J is the asymmetry parameter, $\sigma_J = 0.07$ for $f < f_p$ and $\sigma_J = 0.09$ for $f > f_p$. The
 122 peak enhancement factor $\gamma = 3.3$ is fixed during the campaign. In total, 11 incident wave
 123 conditions were chosen according to preliminary numerical investigations of the UWO setup
 124 (results not shown here). These wave conditions are tested in the experimental wave flume
 125 for the UWO setup. The key parameters of the measurements are listed in Tab. 1, including
 126 the peak period T_p , the significant wave height $H_s = 4\sqrt{m_0}$ (m_0 denoting the zero-th moment
 127 of the wave spectrum), the wave steepness $\epsilon = k_p a$ ($a = \sqrt{2m_0}$, and k_p is the wave number
 128 corresponding to the peak period), and the relative water depth $\mu = k_p h$, averaged over the
 129 upstream flat area or the bar crest area. Note that values of the Ursell number $Ur = \epsilon/\mu^3$ are
 130 not added in Tab. 1 to limit the table size, but they can be easily calculated with the given
 131 values of ϵ and μ .

132 In the UWO tests, k_p is obtained from the peak frequency $\omega_p = 2\pi f_p$ by solving the
 133 dispersion relationship of linear waves:

$$134 \quad \omega = 2\pi/T = \sqrt{gk \tanh(kh)}. \quad (2.2)$$

135 For each condition, 5 wave sequences with 10 min duration each were generated using
 136 different sets of random phases. For particular cases, we have tested 10 wave sequences
 137 with random phases. The evolution trends of the statistical parameters are quite similar to
 138 those obtained with 5 sequences, we therefore anticipate that the results of 5 sequences have
 139 reached or are close to statistical convergence. For all the cases considered in this work, the
 140 values of incident steepness are set moderate, such that no breaking occurs over the bar, even
 141 when freak waves appear.

142 These cases are of relative water depth below or around the transition depth, which was
 143 estimated according to the preliminary numerical study, and the NED is expected to manifest

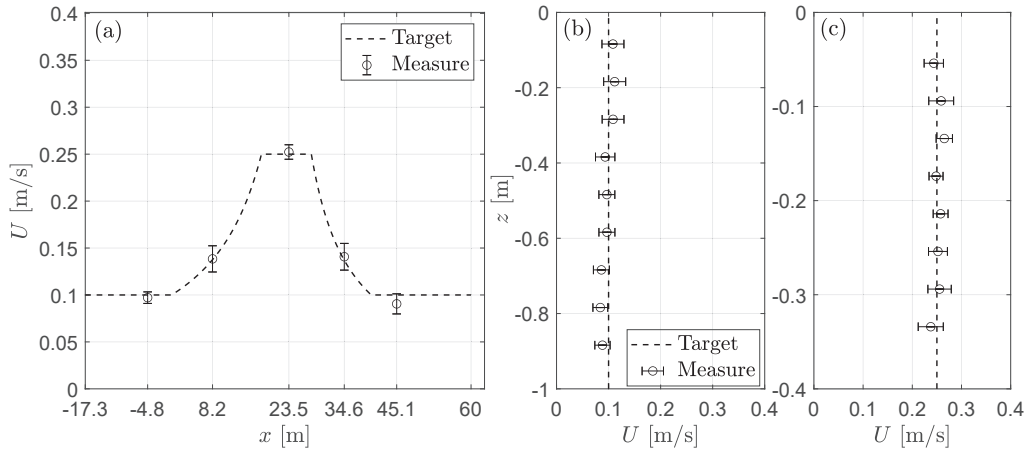


Figure 2: Mean horizontal flow velocity U measured in the UCO setup, (a) longitudinal evolution along the flume, and vertical profiles measured at two abscissas (b) $x = -4.8$ m (before the bar) and (c) $x = 23.5$ m (on the bar crest).

144 in the UWO tests. It should be mentioned that, in the preliminary numerical investigation,
 145 the transition depth for the occurrence of NED in the UWO setup is about 0.9, considerably
 146 smaller than the 1.3 value reported in Trulsen *et al.* (2020). It is conjectured that the difference
 147 in the transition depth is mainly related to the up-slope gradient 1/30 used in this study, which
 148 is significantly smaller than the 1/3.81 slope in Trulsen *et al.* (2020).

149 The same incident wave trains of cases 1–9 were then tested under the UWC condition.
 150 The target current is uniform in the vertical direction yet varying in the horizontal due to
 151 the presence of the bar. The flow velocity U is set to 0.1 m/s in the upstream flat area, and
 152 the corresponding volume flux is $Q = Ubh_1 = 0.15$ m³/s. Considering the conservation of
 153 Q along the flume, the local target flow velocity can be determined as $U(x) = Q/(bh(x))$.
 154 For validation, the UCO tests were conducted before UWC tests, the horizontal flow velocity
 155 was measured with a ‘Vectrino’ Acoustic Doppler Velocimeter (ADV) from Nortek with
 156 sampling frequency 20 Hz. These flow measurements lasted for 10 min after the current
 157 became steady. Fig. 2(a) shows the spatial evolution of the mean horizontal flow velocity
 158 with the standard deviation represented by error bars, Fig. 2(b–c) present the vertical profiles
 159 of horizontal flow velocity at two locations (before the bar and over the bar crest). The
 160 profiles of the target flow velocity are superimposed for comparison. These results indicate
 161 the current was generated as desired.

162 Then, the UWC tests were performed. The key parameters of UWC tests are also given in
 163 Tab. 1, with k_p determined now via the Doppler-shifted dispersion relationship (Peregrine
 164 1976):

$$165 \quad \omega = \sigma + kU = \sqrt{gk \tanh(kh)} + kU, \quad (2.3)$$

166 where σ denotes the intrinsic wave frequency, and taking the lowest of the two positive roots
 167 for k .

168 In the end, the wave trains of cases 1–9 were tested under FWO condition (with uniform
 169 depth h_1). The key parameters of the FWO tests are approximately equal to those in the
 170 upstream flat area of the UWO tests shown in Tab. 1, thus not duplicated.

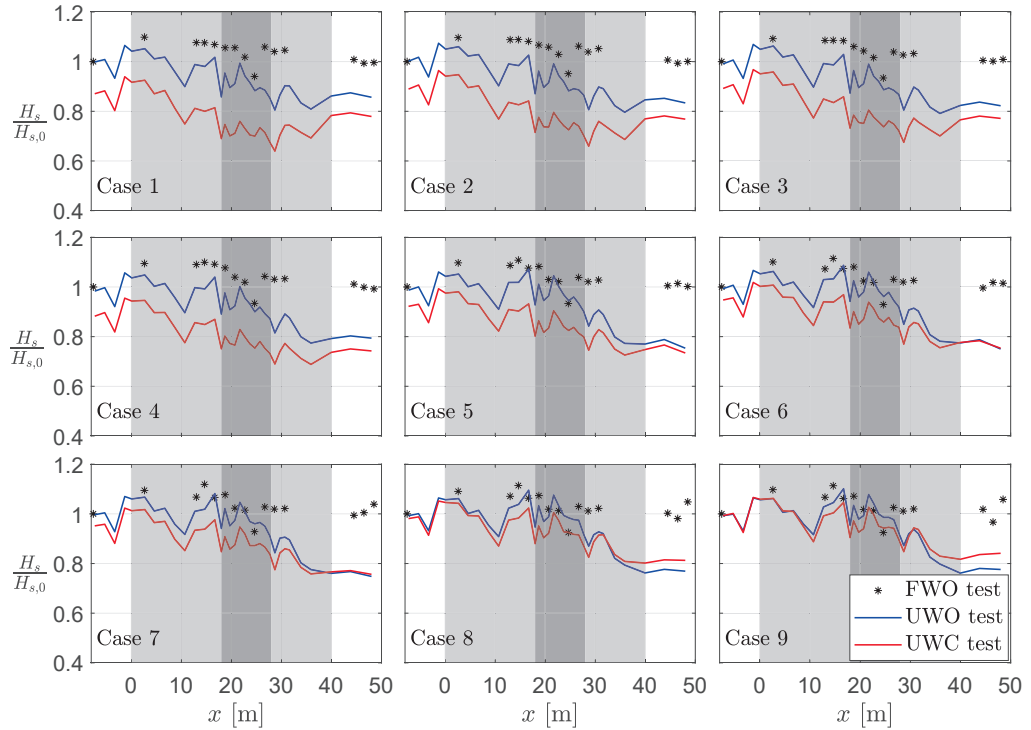


Figure 3: Evolution of normalized significant wave height $H_s/H_{s,0}$ in cases 1–9 for FWO, UWO and UWC setups, with the bar profile indicated by gray areas.

171 3. Results and analysis

172 3.1. Effects of accelerating following current on wave statistics

173 We focus on the effects induced by the current field in addition to effects of the variable
 174 seabed. The results shown are the mean of 5 samples in each case. The spatial evolution of
 175 three statistical parameters are shown, the significant wave height H_s , normalized by $H_{s,0}$,
 176 the significant wave height measured at the first probe of the corresponding FWO case,
 177 skewness $\lambda_3(\eta) = \langle(\eta - \langle\eta\rangle)^3\rangle/m_0^{3/2}$ and kurtosis $\lambda_4(\eta) = \langle(\eta - \langle\eta\rangle)^4\rangle/m_0^2$, with $\langle\cdot\rangle$ being
 178 the averaging operator. Skewness is a measure of wave profile asymmetry in the vertical
 179 direction, and kurtosis is positively correlated with the freak wave occurrence probability.
 180 The local enhancements of these two parameters are seen as the sign of NEP as waves
 181 propagate in non-homogeneous media.

182 Cases 1–9 are tested in the FWO, UWO and UWC scenarios. In Fig. 3, it is shown that
 183 the evolution of $H_s/H_{s,0}$ modulates within a limited range around the mean level, with no
 184 obvious decay in the FWO cases (black asterisks), indicating that the dissipation is negligible
 185 in such circumstances. However, the dissipation is non-trivial in the uneven bottom setup,
 186 H_s is decreased by roughly 20% after the bar in both UWO and UWC tests. The presence of
 187 a following current reduces H_s in comparison to the tests without current, and the reduction
 188 of H_s becomes less evident for longer waves, but more evident for shallower water depth
 189 where the current velocity is increased up to 0.25 m/s. This can be explained by the principle
 190 of wave action conservation (Bretherton & Garrett 1969).

191 Fig. 4 shows the evolution of λ_3 . We see in all the FWO tests, λ_3 remains about 0 throughout
 192 the flume, as expected in a Gaussian sea-state. In both UWO and UWC tests, cases 4–9 show

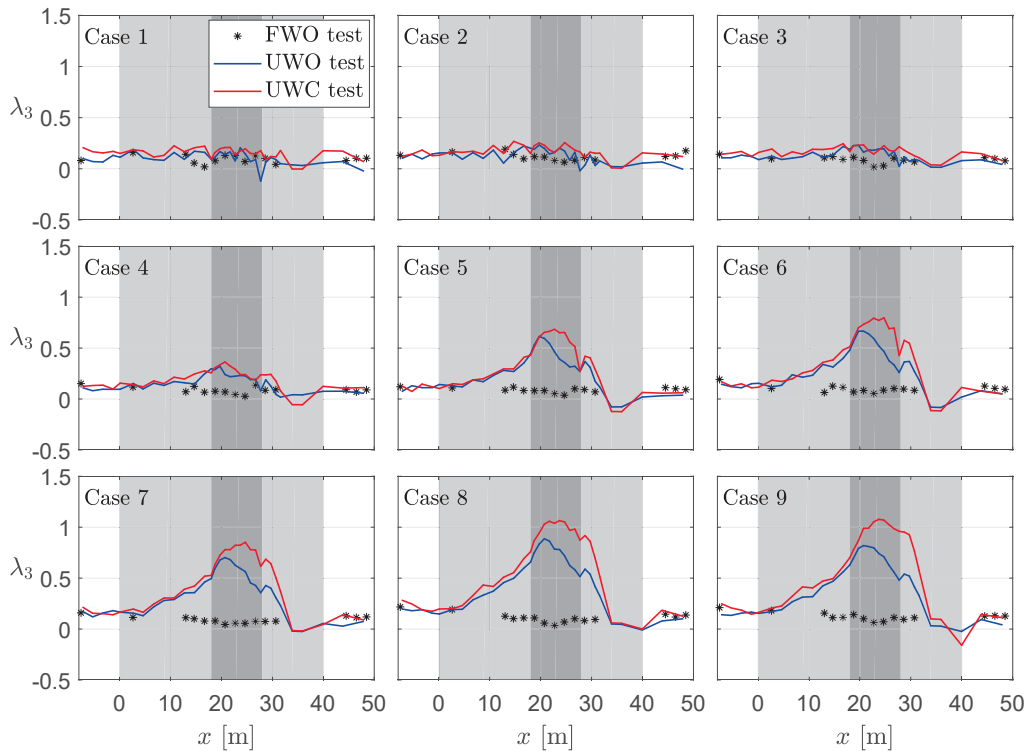


Figure 4: Evolution of skewness λ_3 in cases 1–9 for FWO, UWO and UWC setups, with the bar profile indicated by gray areas.

193 evident local increase of λ_3 , indicating the manifestation of NED over the bar crest. We
 194 notice that the following current further enhances the maximum value of λ_3 (see the red
 195 curves), and extends the region where λ_3 is enhanced. Besides, the spatial extent of the non-
 196 equilibrium area in the UWC tests increases for longer waves. In other words, a following
 197 current increases both the magnitude and the range of NED.

198 The evolution of λ_4 is shown in Fig. 5. The same trends as for λ_3 apply for λ_4 . It is observed
 199 that in cases 3 and 4, the values of λ_4 get locally enhanced over the bar with the following
 200 current, whereas no such increase is noticeable in the corresponding UWO tests. For cases
 201 5–9, the NEP is stronger in magnitude and lasts longer in space in the UWC scenario, in
 202 comparison to the UWO tests. Take case 8 as an example, the maximum value of λ_4 is
 203 increased from 4.3 in the UWO setup upto 5.0 in the UWC setup. This would imply a heavier
 204 tail in the wave height distribution, and therefore a higher freak wave probability.

205 It should be noticed that MI is not responsible for the local increase of λ_3 and λ_4 in
 206 this study. For the UWC tests, in the upstream flat area with $h_1 = 1$ m and $U_1 = 0.1$ m/s,
 207 the MI is expected to manifest for $k_p h_1 > 1.39$; over the bar crest with $h_2 = 0.4$ m and
 208 $U_2 = 0.25$ m/s, the threshold for MI increases to $k_p h_2 > 1.48$ (see eq. (41) in Liao *et al.*
 209 2017). For the UWO tests, the $k_p h$ threshold for MI is always 1.36. Therefore, waves in all
 210 cases are modulationally stable over the bar crest.

211 Undoubtedly, the UWC setup considered in this study is complicated, involving wave-
 212 wave, wave-bottom, wave-current and current-bottom interactions. Based on the analysis of
 213 the threshold water depth with current effect taken into account, the MI is considered to be
 214 insignificant for the local increase of skewness and kurtosis over the bar crest. The uneven

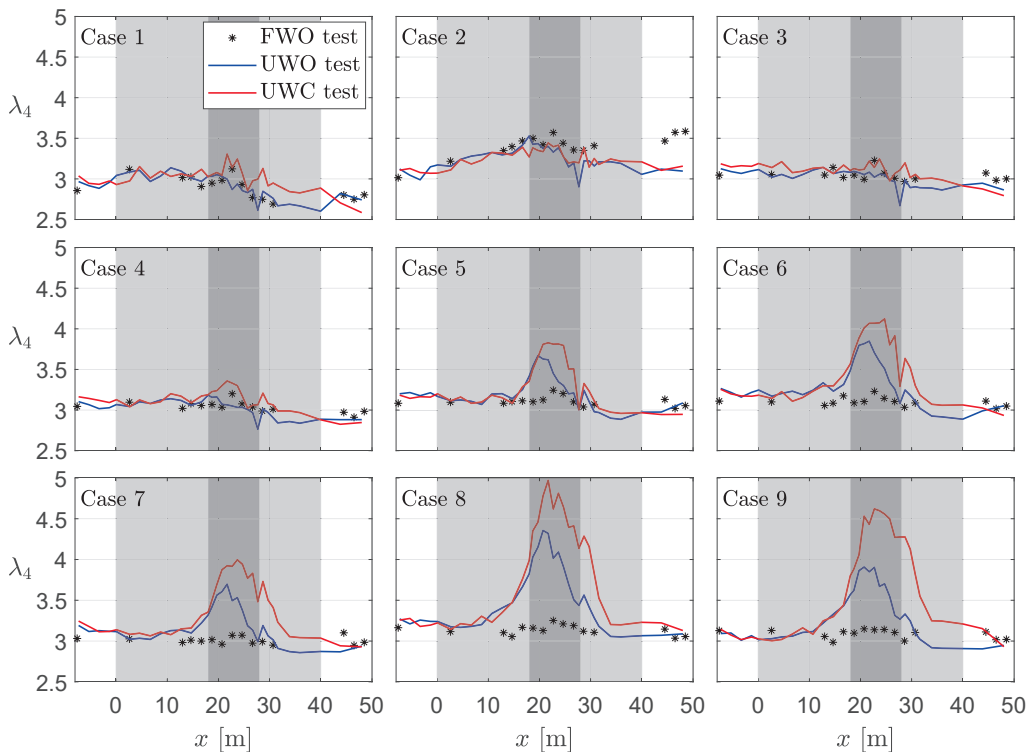


Figure 5: Evolution of kurtosis λ_4 in cases 1–9 for FWO, UWO and UWC setups, with the bar profile indicated by gray areas.

215 bottom could increase the vorticity of the fluid, but this could be omitted considering the
 216 gentleness of the slope.

217 The uneven bottom might also give rise to free surface deformation when a pure (steady)
 218 current passes over, as a result of significant current-bottom interaction (see e.g. Buttle *et al.*
 219 2018; Akselsen & Ellingsen 2019). It should be pointed out that such current-induced free
 220 surface deformation (CIFSD) is a steady solution, i.e., the CIFSD is time-independent when
 221 the steady state is achieved. The CIFSD can therefore be considered as a change of the local
 222 mean water level, resulting in a change of the local water depth. The wave evolution may
 223 therefore be influenced by the CIFSD. In the present study, the current was generated 10 min
 224 before the wave-paddle started to move, so the steady state of the flow field was achieved,
 225 and the steady profile of the CIFSD over the bar crest was well established. Following
 226 eq. (2.4) in Buttle *et al.* (2018), the maximum magnitude of CIFSD is about 0.003 m for our
 227 experimental tests. As it represents a very small variation of the water depth over the bar crest
 228 ($0.003/h_2 < 1\%$), we consider that the contribution of CIFSD to the evolution of central
 229 moments like skewness and kurtosis is minor and can be safely neglected in our study. In all,
 230 it is considered that the presence of the uneven bottom gradually changes the mean horizontal
 231 flow velocity without changing the (near) uniformity of the horizontal flow velocity along
 232 z -axis, and that the occurrence of CIFSD does not contribute to the local changes of λ_3 and
 233 λ_4 over the bar.

234 We understand the accelerating following current enhances and extends the local increase
 235 of λ_3 and λ_4 as follows: a following current affects the surface waves in two folds, on one
 236 hand, it decreases the significant wave height (conservation of wave action), on the other

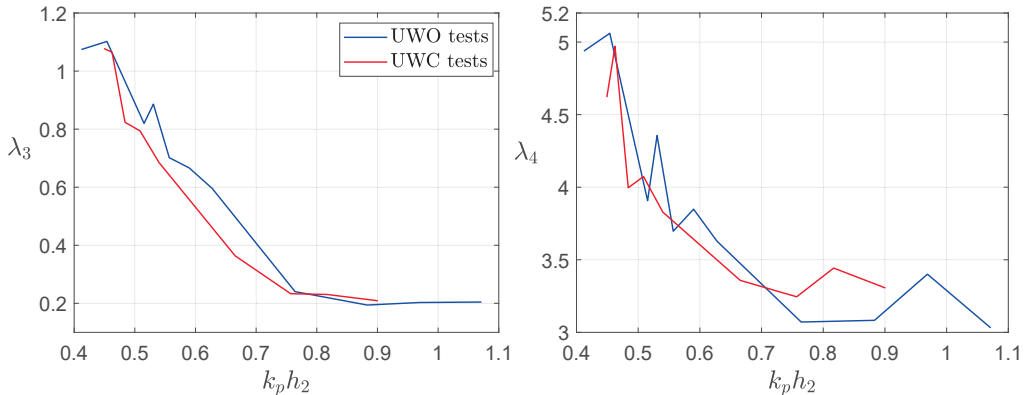


Figure 6: Maximum values of skewness (left) and kurtosis (right) over the shallower region as a function of the relative water depth over the bar crest.

237 hand, it decreases the wave number (Doppler effect). Both the steepness ϵ and the relative
 238 water depth μ are therefore decreased. The relative water depth over the shallower region
 239 $k_p h_2$ plays a dominant role in the manifestation of NED, smaller $k_p h_2$ results in stronger
 240 NEP. Thus, it is understandable to observe higher levels of λ_3 and λ_4 . Compared to the UWO
 241 tests, the following current in the UWC tests increases the level of media inhomogeneity, a
 242 longer spatial distance is needed for the sea-state to adapt to the new equilibrium state.

243 3.2. Saturation depth for the maximum values of skewness and kurtosis

244 Fig. 6 further illustrates the relationship between the maximum values of λ_3 , λ_4 (representing
 245 the magnitude of the NED) and the relative water depth $k_p h_2$ over the bar crest. The blue
 246 curve contains all 11 cases under UWO condition, and the red curve contains cases 1–9
 247 under the UWC condition. Values of k_p are computed with the current velocity taken into
 248 account (using eq. (2.3)). It is shown that, the evolution trends of maximum values of λ_3 , λ_4
 249 as functions of $k_p h_2$ are very similar in UWO and UWC scenarios (given k_p computed with
 250 proper dispersion relation). In our experiments, the NEP starts to appear for $k_p h_2 \approx 0.8$ (the
 251 above-mentioned “transition” depth).

252 Furthermore, Fig. 6 shows that the increase of λ_3 and λ_4 with the decrease of $k_p h_2$
 253 seems to stop for $k_p h_2 \approx 0.45$. This is not surprising since the increase trend of λ_3 and λ_4
 254 cannot sustain unlimitedly. We refer to this particular relative water depth $k_p h_2 \approx 0.45$ as the
 255 “saturation depth” of the NED. Below that saturation depth, λ_3 and λ_4 will no longer increase
 256 with a decrease of $k_p h_2$. As the peak period T_p increases, the relative water depth decreases
 257 throughout the flume. The difference between the shallower and the deeper depth (i.e. the
 258 change of condition) also reduces, therefore the non-equilibrium responses are weakened,
 259 the increase trends of λ_3 and λ_4 slow down as well.

260 The saturation depth has been indicated (without defining a terminology) in the theoretical
 261 work of Mendes *et al.* (2022), where these authors consider the enhancement of λ_3 and
 262 λ_4 takes place for $k_p h_2 \in [0.5, 1.5]$. Yet, such a saturation depth has never been reported
 263 in experimental works. It is anticipated that as the water depth decreases further, the wave
 264 evolution would be dominated by other effects, such as shallow water effect and depth-
 265 induced breaking effect. Investigating these effects is certainly of academic and practical
 266 significance, yet it is beyond the present discussion of NED.

267 To further illustrate the “saturation” effects, Fig. 7 superimposes the evolution of λ_3 and
 268 λ_4 in four cases, cases 8 and 9 in the UWC scenario, and cases 10 and 11 in the UWO
 269 scenario. In all these cases, $k_p h_2$ is considered saturated. It can be observed that the spatial

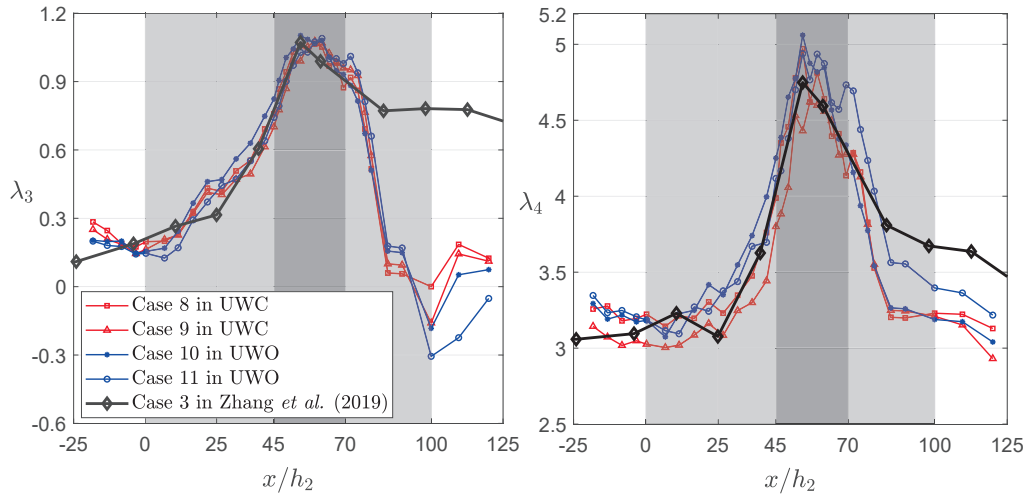


Figure 7: Evolution of skewness (left) and kurtosis (right) in cases 8–11, and in case 3 reported in Zhang *et al.* (2019). In all cases, $k_p h_2$ is below the saturation depth.

270 profiles of λ_3 and λ_4 are very similar in these cases. Especially, the evolution of λ_3 is almost
 271 identical. When $k_p h_2$ saturates, in addition to similar maximum values of λ_3 and λ_4 , we
 272 also notice that the following current does not result in a longer spatial range of NED. As
 273 a cross-validation for the saturation depth, we add in this Fig. 7 one of the experimental
 274 results of Zhang *et al.* (2019), obtained in a wave flume of Tainan Hydraulics Laboratory
 275 (THL). In the THL experiments, the bathymetry is composed of two flat regions connected
 276 by a constant up-slope (1/20). Here, we only take the case 3 reported in Zhang *et al.* (2019),
 277 in which $k_p h_2$ happens to be 0.45 ($T_p = 2.5$ s, $h_2 = 0.3$ m, no current). In Fig. 7, the
 278 evolution of λ_3 and λ_4 of THL-case 3 in Zhang *et al.* (2019) (black curves) is shifted in
 279 space, so that the positions of maximum λ_3 and λ_4 align with the present results. Despite
 280 considerably different configurations, the spatial profiles of λ_3 and λ_4 in THL-case 3 are in
 281 good agreement with the present results. It should be understood that λ_3 keeps a high level
 282 after 30 m in THL-case 3 because there is no de-shoaling process. Therefore, we speculate the
 283 saturation depth $k_p h_2 \approx 0.5$ has some universal relevance, though this needs to be confirmed
 284 by additional investigations.

285 4. Conclusion

286 We experimentally investigated the non-equilibrium dynamics (NED) of surface waves
 287 induced by medium inhomogeneity, here provoked by spatially varying water depth and
 288 current velocity. In this experimental campaign, 11 irregular wave conditions have been
 289 tested under FWO, UWO and UWC scenarios. The results show that a following current
 290 could amplify the medium inhomogeneity as waves propagate over a shoal, such that higher
 291 peaks and wider spatial extents of the local enhancement of skewness λ_3 and kurtosis λ_4
 292 are achieved. The probability of freak waves is therefore enhanced due to an accelerating
 293 following current. This is because the decrease of the relative water depth can overwhelm
 294 the decrease of wave steepness, resulting in stronger sea-state non-equilibrium dynamical
 295 response over a larger spatial extent. The maximum values of λ_3 and λ_4 achieved over the
 296 bar crest increase with the decrease of $k_p h_2$ in the UWO tests, and the relationships hold for
 297 the UWC tests with k_p evaluated with the current velocity taken into account.

298 The evolution of maximum λ_3 , λ_4 as functions of $k_p h_2$ shows two particular thresholds

299 of relative depth: one is the so-called “transition depth” (Trulsen *et al.* 2020), below which
 300 the NED starts to manifest (about 0.8 in our experimental setup); the other one is about
 301 0.45 – 0.5, below which the maximum λ_3 and λ_4 no longer increase with a further decrease
 302 of $k_p h_2$, the latter is named “saturation depth”. To the limit of our knowledge, this saturation
 303 depth has never been reported in previous experimental works.

304 The present results are of high practical importance, especially for the assessment of freak
 305 wave risks in coastal areas with ambient currents. We have demonstrated that, somewhat
 306 counter-intuitively, a following current entering a shallow water area increases the risk of
 307 extreme waves in this area.

308 Acknowledgements

309 This work was supported by the National Natural Science Foundation of China (Grants
 310 No. 52101301; 51720105010), the China Postdoctoral Science Foundation (Grant No.
 311 2021M690523) and the Innovative Research Foundation of Ship General Performance (Grant
 312 No. 31422119). The authors are grateful to the three anonymous reviewers for their valuable
 313 suggestions on various aspects that have considerably improved the manuscript, in particular
 314 on the discussion of CIFSD.

315 Declaration of interests

316 The authors report no conflict of interest.

REFERENCES

- 317 ADCOCK, T. A. A. & TAYLOR, P. H. 2014 The physics of anomalous (‘rogue’) ocean waves. *Rep. Prog. Phys.*
 318 **77**, 105901.
- 319 AKHMEDIEV, N. & PELINOVSKY, E. 2010 Editorial – introductory remarks on “discussion & debate: Rogue
 320 waves – towards a unifying concept?”. *Eur. Phys. J.: Spec. Top* **185**, 1–4.
- 321 AKSELSEN, A. H. & ELLINGSEN, S. Å. 2019 Sheared free-surface flow over three-dimensional obstructions
 322 of finite amplitude. *J. Fluid Mech.* **878**, 740–767.
- 323 BENJAMIN, T. B. 1967 Instability of periodic wavetrains in nonlinear dispersive systems. *Proc. R. Soc. A:*
 324 *Math. Phys. Eng. Sci.* **299**, 59–76.
- 325 BRETHERTON, F. P. & GARRETT, C. J. R. 1969 Wavetrains in inhomogeneous moving media. *Proc. Math.*
 326 *Phys. Eng. Sci.* **302**, 529–554.
- 327 BUTTLE, N. R., PETHIYAGODA, R., MORONEY, T. J. & McCUE, S. W. 2018 Three-dimensional free-surface
 328 flow over arbitrary bottom topography. *J. Fluid Mech.* **846**, 166–189.
- 329 CHAWLA, A. & KIRBY, J. T. 2002 Monochromatic and random wave breaking at blocking points. *J. Geophys.*
 330 *Res.* **107**, 3067.
- 331 CURTIS, C. W. & MURPHY, M. 2020 Evolution of spectral distributions in deep-water constant vorticity
 332 flows. *Water Waves* **2**, 361–380.
- 333 DEMATTEIS, G., GRAFKE, T., ONORATO, M. & VANDEN-EIJNDEN, E. 2019 Experimental evidence of
 334 hydrodynamic instantons: The universal route to rogue waves. *Phys. Rev. X* **9**, 041057.
- 335 DUCROZET, G., ABDOLAHPOUR, M., NELLI, F. & TOFFOLI, A. 2021 Predicting the occurrence of rogue waves
 336 in the presence of opposing currents with a high-order spectral method. *Phys. Rev. Fluids* **6**, 064803.
- 337 DUCROZET, G. & GOUIN, M. 2017 Influence of varying bathymetry in rogue wave occurrence within
 338 unidirectional and directional sea-states. *J. Ocean Eng. Mar. Energy* **3**, 309–324.
- 339 DYSTHE, K., KROGSTAD, H. E. & MÜLLER, P. 2008 Oceanic rogue waves. *Annu. Rev. Fluid Mech.* **40**,
 340 287–310.
- 341 FEDELE, F., BRENNAN, J., PONCE DE LEÓN, S., DUDLEY, J. & DIAS, F. 2016 Real world ocean rogue waves
 342 explained without the modulational instability. *Sci. Rep.* **6**, 27715.
- 343 GERBER, M. 1987 The Benjamin-Feir instability of a deep-water Stokes wavepacket in the presence of a
 344 non-uniform medium. *J. Fluid Mech.* **176**, 311–332.

- 345 GRAMSTAD, O., ZENG, H., TRULSEN, K. & PEDERSEN, G. K. 2013 Freak waves in weakly nonlinear
346 unidirectional wave trains over a sloping bottom in shallow water. *Phys. Fluids* **25**, 122103.
- 347 HJELMERVIK, K. B. & TRULSEN, K. 2009 Freak wave statistics on collinear currents. *J. Fluid Mech.* **637**,
348 267–284.
- 349 KASHIMA, H. & MORI, N. 2019 Aftereffect of high-order nonlinearity on extreme wave occurrence from
350 deep to intermediate water. *Coastal Eng.* **153**, 103559.
- 351 KHARIF, C., KRAENKEL, R. A., MANNA, M. A. & THOMAS, R. 2010 The modulational instability in deep
352 water under the action of wind and dissipation. *J. Fluid Mech.* **664**, 138–149.
- 353 KHARIF, C. & PELINOVSKY, E. 2003 Physical mechanisms of the rogue wave phenomenon. *Eur. J. Mech. B.*
354 *Fluids* **22**, 603–634.
- 355 LAVRENOV, I. V. & PORUBOV, A. V. 2006 Three reasons for freak wave generation in the non-uniform current.
356 *Eur. J. Mech. B. Fluids* **25**, 574–585.
- 357 LAWRENCE, C., TRULSEN, K. & GRAMSTAD, O. 2021 Statistical properties of wave kinematics in long-crested
358 irregular waves propagating over non-uniform bathymetry. *Phys. Fluids* **33**, 046601.
- 359 LAWRENCE, C., TRULSEN, K. & GRAMSTAD, O. 2022 Extreme wave statistics of surface elevation and velocity
360 field of gravity waves over a two-dimensional bathymetry. *J. Fluid Mech.* **939**, A41.
- 361 LI, Y., DRAYCOTT, S., ADCOCK, T. A. A. & VAN DEN BREMER, T. S. 2021a Surface wavepackets subject to an
362 abrupt depth change. Part 2. experimental analysis. *J. Fluid Mech.* **915**, A72.
- 363 LI, Y., DRAYCOTT, S., ZHENG, Y., LIN, Z., ADCOCK, T. A. A. & VAN DEN BREMER, T. S. 2021b Why rogue
364 waves occur atop abrupt depth transitions. *J. Fluid Mech.* **919**, R5.
- 365 LI, Y., ZHENG, Y., LIN, Z., ADCOCK, T. A. A. & VAN DEN BREMER, T. S. 2021c Surface wavepackets subject
366 to an abrupt depth change. Part 1. second-order theory. *J. Fluid Mech.* **915**, A71.
- 367 LIAO, B., DONG, G., MA, Y. & GAO, J. L. 2017 Linear-shear-current modified Schrödinger equation for
368 gravity waves in finite water depth. *Phys. Rev. E* **96**, 043111.
- 369 LONGUET-HIGGINS, M. S. & STEWART, R. W. 1961 The changes in amplitude of short gravity waves on steady
370 non-uniform currents. *J. Fluid Mech.* **10**, 529–549.
- 371 MA, Y., CHEN, H., MA, X. & DONG, G. 2017 A numerical investigation on nonlinear transformation of
372 obliquely incident random waves on plane sloping bottoms. *Coastal Eng.* **130**, 65–84.
- 373 MA, Y., DONG, G., PERLIN, M., MA, X., WANG, G. & XU, J. 2010 Laboratory observations of wave evolution,
374 modulation and blocking due to spatially varying opposing currents. *J. Fluid Mech.* **661**, 108–129.
- 375 MA, Y., MA, X. & DONG, G. 2015 Variations of statistics for random waves propagating over a bar. *J. Mar.*
376 *Sci. Technol.* **23**, 864–869.
- 377 MENDES, S., SCOTTI, A., BRUNETTI, M. & KASPARIAN, J. 2022 Non-homogeneous analysis of rogue wave
378 probability evolution over a shoal. *J. Fluid Mech.* **939**, A25.
- 379 ONORATO, M., PROMENT, D. & TOFFOLI, A. 2011 Triggering rogue waves in opposing currents. *Phys. Rev.*
380 *Lett.* **107**, 184502.
- 381 ONORATO, M., RESIDORI, S., BORTOLOZZO, U., MONTINA, A. & ARECCHI, F. T. 2013 Rogue waves and their
382 generating mechanisms in different physical contexts. *Phys. Rep.* **528**, 47–89.
- 383 ONORATO, M. & SURET, P. 2016 Twenty years of progresses in oceanic rogue waves: the role played by
384 weakly nonlinear models. *Nat. Hazards* **84**, 541–548.
- 385 PEREGRINE, D. H. 1976 Interaction of water waves and currents. In *Advances in Applied Mechanics*, pp.
386 9–117. Elsevier.
- 387 STOCKER, J. R. & PEREGRINE, D. H. 1999 The current-modified nonlinear schrödinger equation. *J. Fluid*
388 *Mech.* **399**, 335–353.
- 389 TOFFOLI, A., CAVALERI, L., BABANIN, A. V., BENOIT, M., BITNER-GREGENSEN, E. M., MONBALIU, J.,
390 ONORATO, M., OSBORNE, A. R. & STANSBERG, C. T. 2011 Occurrence of extreme waves in three-
391 dimensional mechanically generated wave fields propagating over an oblique current. *Nat. Hazards*
392 *Earth Syst. Sci.* **11**, 895–903.
- 393 TOFFOLI, A., FERNANDEZ, L., MONBALIU, J., BENOIT, M., GAGNAIRE-RENOU, E., LEFÈVRE, J. M., CAVALERI,
394 L., PROMENT, D., PAKOZDI, C., STANSBERG, C. T., WASEDA, T. & ONORATO, M. 2013 Experimental
395 evidence of the modulation of a plane wave to oblique perturbations and generation of rogue waves
396 in finite water depth. *Phys. Fluids* **25**, 091701.
- 397 TOFFOLI, A., WASEDA, T., HOUTANI, H., CAVALERI, L., GREAVES, D. & ONORATO, M. 2015 Rogue waves in
398 opposing currents: an experimental study on deterministic and stochastic wave trains. *J. Fluid Mech.*
399 **769**, 277–297.
- 400 TRULSEN, K. 2018 Rogue waves in the ocean, the role of modulational instability, and abrupt changes of

- 401 environmental conditions that can provoke non equilibrium wave dynamics. In *The Ocean in Motion*,
402 pp. 239–247. Springer International Publishing.
- 403 TRULSEN, K., RAUSTØL, A., JORDE, S. & RYE, L. B. 2020 Extreme wave statistics of long-crested irregular
404 waves over a shoal. *J. Fluid Mech.* **882**, R2.
- 405 TRULSEN, K., ZENG, H. & GRAMSTAD, O. 2012 Laboratory evidence of freak waves provoked by non-uniform
406 bathymetry. *Phys. Fluids* **24**, 097101.
- 407 VORONOVICH, V. V., SHRIRA, V. I. & THOMAS, G. 2008 Can bottom friction suppress ‘freak wave’ formation?
408 *J. Fluid Mech.* **604**, 263–296.
- 409 WHITE, B. S. & FORNBERG, B. 1998 On the chance of freak waves at sea. *J. Fluid Mech.* **355**, 113–138.
- 410 ZENG, H. & TRULSEN, K. 2012 Evolution of skewness and kurtosis of weakly nonlinear unidirectional waves
411 over a sloping bottom. *Nat. Hazards Earth Syst. Sci.* **12**, 631–638.
- 412 ZHANG, J. & BENOIT, M. 2021 Wave–bottom interaction and extreme wave statistics due to shoaling and
413 de-shoaling of irregular long-crested wave trains over steep seabed changes. *J. Fluid Mech.* **912**,
414 A28.
- 415 ZHANG, J., BENOIT, M., KIMMOUN, O., CHABCHOUB, A. & HSU, H.-C. 2019 Statistics of extreme waves in
416 coastal waters: large scale experiments and advanced numerical simulations. *Fluids* **4**, 99.
- 417 ZHANG, J., BENOIT, M. & MA, Y. 2022 Equilibration process of out-of-equilibrium sea-states induced by
418 strong depth variation: Evolution of coastal wave spectrum and representative parameters. *Coastal*
419 *Eng.* **174**, 104099.
- 420 ZHENG, Y., LIN, Z., LI, Y., ADCOCK, T. A. A., LI, Y. & VAN DEN BREMER, T. S. 2020 Fully nonlinear
421 simulations of unidirectional extreme waves provoked by strong depth transitions: The effect of
422 slope. *Phys. Rev. Fluids* **5**, 064804.